CMS Physics Analysis Summary

Contact: cms-pag-conveners-heavyions@cern.ch 2015/06/30

Suppression of Y(1S), Y(2S) and Y(3S) in PbPb collisions at $\sqrt{s_{\mathrm{NN}}} = 2.76$ TeV

The CMS Collaboration

Abstract

Yields of Y(1S), Y(2S) and Y(3S) mesons are measured in the CMS experiment via their $\mu^+\mu^-$ decays, for bottomonium rapidity $|y| < 2.4$, in PbPb and pp collisions at the same energy, $\sqrt{s_{\mathrm{NN}}} = 2.76$ TeV. The CMS detector was used to collect integrated luminosity of 166 $\mu\mathrm{b}^{-1}$ for PbPb and 5.4 pb^{-1} for pp, corresponding to a similar total number of nucleon-nucleon collisions. Differential cross sections and nuclear modification factors are reported as functions of rapidity and transverse momentum, as well as collision centrality, for the Y(1S) and the Y(2S). By comparing to the yield in pp collisions scaled by the number of inelastic nucleon-nucleon collisions, a strong, centrality-dependent suppression is observed in PbPb collisions, by up to a factor of 2 and 10, for the Y(1S) and the Y(2S), respectively. No significant dependences are observed as functions of rapidity or transverse momentum. The Y(3S) was not observed in PbPb collisions, being suppressed by more than 7 at the 95% confidence level.

1 Introduction

At large energy densities and high temperatures, strongly interacting matter consists of a deconfined and chirally-symmetric system of quarks and gluons [1]. This state, often referred to as "quark-gluon plasma" (QGP) [2], constitutes the main object of the studies performed with relativistic heavy-ion collisions.

The formation of a QGP in high-energy nuclear collisions can be evidenced in a variety of ways. One of the most striking expected signatures is the suppression of quarkonium states [3], both of the charmonium (J/ψ, ψ', χ_c, etc.) and the bottomonium (Υ(1S, 2S, 3S), χ_b, etc.) families. This is thought to be a direct effect of deconfinement, when the binding potential between the constituents of a quarkonium state, a heavy quark and its antiquark, is screened by the colour charges of the surrounding light quarks and gluons. The suppression is predicted to occur above the critical temperature of the medium (T_c) and depends on the $\mathrm{Q\overline{Q}}$ binding energy. Since the Υ(1S) is the most tightly bound state among all quarkonia, it is expected to be the one with the highest dissociation temperature. Examples of dissociation temperatures are given in Ref. [4]: $T_{\mathrm{dissoc}} \sim 1\,T_c$, $1.2\,T_c$, and $2\,T_c$ for the Υ(3S), Υ(2S), and Υ(1S), respectively. However, there are further possible changes to the quarkonium production in the hot expanding medium created in heavy ion collisions, such as regeneration of initially-uncorrelated quark-antiquark pairs [5, 6] or absorption by comoving particles [7, 8]. Furthermore, nuclear effects such as modifications to the parton distribution functions inside the nucleus (shadowing) are expected to reduce the production of quarkonia regardless of the QGP formation [9]. An admixture of the above-mentioned effects in the context of bottomonia production is investigated in Ref. [10].

The suppression of the Υ(1S) in heavy-ion collisions was first measured by the CMS collaboration [11]. The suppression of the Υ(2S) and Υ(3S) was also first suggested [12] then observed [13] by CMS. In pPb collisions, the ALICE [14] and LHCb [15] collaborations reported Υ(1S) yields that are slightly lower than the binary-scaled yields extrapolated from pp collisions at different energies, in the p-going forward direction. The Υ(2S) and Υ(3S) were reported by the CMS collaboration to be slightly more suppressed than the Υ(1S) in pPb collisions [16].

In this document, the yields of Υ(1S), Υ(2S) and Υ(3S) mesons are reported, from PbPb and pp data sets at the same center-of-mass energy of $\sqrt{s_{\mathrm{NN}}} = 2.76$ TeV, corresponding to 166 $\mu\mathrm{b}^{-1}$ and 5.4 pb^{-1}, respectively. With respect to [13], the PbPb data reconstruction was improved yielding an increase of $\approx$ 30% in the Υ(1S) yields. The pp data set, recorded in 2013, is new and allows for further differential studies as functions of the Υ rapidity (y) and transverse momentum (p_{T}). From the PbPb and pp yields, nuclear modification factors, R_{AA}, are derived.

2 The CMS detector

A detailed description of the CMS experiment can be found in Ref. [17]. The central feature of the CMS apparatus is a superconducting solenoid of 6 m internal diameter. Within the field volume are the silicon tracker, the crystal electromagnetic calorimeter, and the brass/scintillator hadron calorimeter.

Muons are detected in the interval $|\eta| < 2.4$ by gaseous detectors made of three technologies: drift tubes, cathode strip chambers, and resistive plate chambers, embedded in the steel return yoke. The silicon tracker is composed of pixel detectors (three barrel layers and two forward disks on either side of the detector, made of 66 million $100 \times 150\,\mu\mathrm{m}^2$ pixels) followed by microstrip detectors (ten barrel layers plus three inner disks and nine forward disks on either side

of the detector, with strips of pitch between 80 and 180 μm). The transverse momentum of muons matched to reconstructed tracks is measured with a resolution better than $\sim$1.5% for p_{T} smaller than 100 GeV/c [18]. The good resolution is the result of the 3.8 T magnetic field and the high granularity of the silicon tracker.

In addition, CMS has extensive forward calorimetry, including two steel/quartz-fibre Cherenkov forward hadron (HF) calorimeters, which cover the pseudorapidity range $2.9 < |\eta| < 5.2$. These detectors are used in the present analysis for the event selection and PbPb collision centrality determination, as described in the next section.

3 Event and muon selections

3.1 Event selection and centrality

In order to select a sample of purely inelastic hadronic PbPb collisions, the contributions from ultraperipheral collisions and non-collision beam background are removed, as described in Ref. [19]. Events are preselected if they contain a reconstructed primary vertex containing at least two tracks and at least three HF towers on each side of the interaction point with an energy of at least 3 GeV deposited in each tower. To further suppress the beam-gas events, the distribution of hits in the pixel detector along the beam direction is required to be compatible with particles originating from the event vertex. These criteria select (97 ± 3)% of inelastic hadronic PbPb collisions [19], corresponding to a number of efficiency-corrected minimum bias (MB) events $N_{\mathrm{MB}} = (1.16 \pm 0.04) \times 10^9$ for the sample analyzed. The pp data set corresponds to an integrated luminosity of 5.4 pb^{-1} known to an accuracy of 3.7% from the uncertainty in the calibration based on a van der Meer scan [20]. The two datasets correspond to approximately the same number of elementary nucleon-nucleon collisions.

The measurements reported here are based on dimuon events triggered by the Level-1 (L1) trigger, a hardware-based trigger that uses information from the muon detectors. No selection is applied on the muon momentum. The CMS detector is also equipped with a software-based high-level trigger (HLT), where fake muons are further rejected. The pp and PbPb data follow the same trigger logic.

The centrality of PbPb collisions is defined as the fraction of the total inelastic hadronic cross section, starting at 0% for the most central collisions. This fraction is determined from the distribution of total energy measured in both HF calorimeters. Using a Glauber-model calculation as described in Ref. [19], one can estimate variables related to the centrality, such as the number of nucleons participating in the collisions (N_{part}) and the nuclear overlap function (T_{AA}) [21]. The latter is equal to the number of elementary nucleon-nucleon (NN) binary collisions divided by the elementary NN cross section and can be interpreted as the NN-equivalent integrated luminosity per heavy ion collision, at a given centrality. The values of these variables are presented in Table 1 for the centrality bins used in this analysis. The uncertainty on T_{AA} is computed by varying the Glauber parameters, as described in Ref. [19]. In the following, N_{part} will be the variable used to show the centrality dependence of the measurements, while T_{AA} directly enters into the nuclear modification factor calculation: $R_{AA} = N_{PbPb}/T_{AA} \times \sigma_{pp}$ where N_{PbPb} is the number of Υ produced per collisions and σ_{pp} the corresponding pp cross section.

3.2 Muon selection

Muons are reconstructed using a global fit to a track in the muon detectors matched to a track in the silicon tracker. The offline muon reconstruction algorithm used for the PbPb data has been

Table 1: Glauber model calculated average values of the number of participating nucleons (N_{part}) and of the nuclear overlap function (T_{AA}) for the centrality bins used in this analysis.

Centrality (%)	N_{part}	T_{AA} (mb^{-1})
0–5	381	25.9 ± 1.1
5–10	329	20.5 ± 0.9
10–20	261	14.5 ± 0.76
20–30	187	8.78 ± 0.58
30–40	130	5.09 ± 0.43
40–50	86.3	2.75 ± 0.30
50–70	42.0	0.985 ± 0.145
70–100	8.75	0.130 ± 0.020
50–100	22.1	0.486 ± 0.073
0–100	113	5.66 ± 0.35

significantly improved relative to that used for the previous measurement [13]. The efficiency has been increased by running multiple iterations in the pattern recognition step, raising the number of reconstructed $\Upsilon(1S)$ by approximately 30%. Background muons from cosmic rays and heavy-quark semileptonic decays are rejected by requiring a set of selection criteria on each muon track. The criteria used are based on previous studies of the performance of the muon reconstruction [22]. To ensure a good p_{T} measurement, more than 10 hits in the tracker are required, and the χ^2 per number of degrees of freedom of the tracker-only (tracker+muon detectors) trajectory fits is required to be less than 4 (10). To further reject cosmic muons and muons from decays in flight, the track is required to have a hit from at least one pixel detector layer and a transverse (longitudinal) distance of closest approach of less than 3 (15) cm from the measured primary vertex position. Pairs of oppositely charged muons are considered dimuon candidates if the χ^2 fit probability of the tracks originating from a common vertex exceeds 1%.

The individual muon-p_{T} are limited to be above 4 GeV/c for the $\Upsilon(2S)$ and $\Upsilon(3S)$ analyses as in previous publications [11–13], while one of them is allowed to go down to 3.5 GeV/c for the $\Upsilon(1S)$. Though this is not beneficial to the significance of the $\Upsilon(2S)$ and $\Upsilon(3S)$ yields, this p_{T}-lowering criterion raises the $\Upsilon(1S)$ yield by $\approx 45\%$, and its significance by up to 50% depending on the dimuon p_{T} and y. The resulting invariant mass distributions for the entire data samples are shown in Fig. 1 for pp and PbPb collisions.

4 Analysis

4.1 Signal extraction

To extract the $\Upsilon(1S)$, $\Upsilon(2S)$ and $\Upsilon(3S)$ yields, unbinned maximum likelihood fits to the $\mu^+\mu^-$ invariant mass spectra are performed between 7.5 and 14 GeV/c^2. The fit results for the p_{T}-, y- and centrality-integrated case are displayed as lines on Fig. 1. The Υ resonances are modelled by the sum of two Crystal Ball (CB) functions, that is, Gaussian resolution functions with the low side tail replaced with a power law describing final state radiation [23]. This choice was suggested by simulation studies, as well as by high-statistics pp analyses $\sqrt{s} = 7$ TeV [24]. Given the relatively large statistical uncertainties of the 2.76 TeV samples, most of the parameters are fixed to values provided by simulations, then allowed to vary to compute the associated systematic uncertainties. Only the $\Upsilon(1S)$ mass, and the $\Upsilon(1S)$, $\Upsilon(2S)$ and $\Upsilon(3S)$ yields are left free. The mass of the $\Upsilon(2S)$ and $\Upsilon(3S)$ are constrained to be equal to the fitted $\Upsilon(1S)$ mass multiplied by the mass ratio from the Particle Data Group [25]. The background is modelled by an

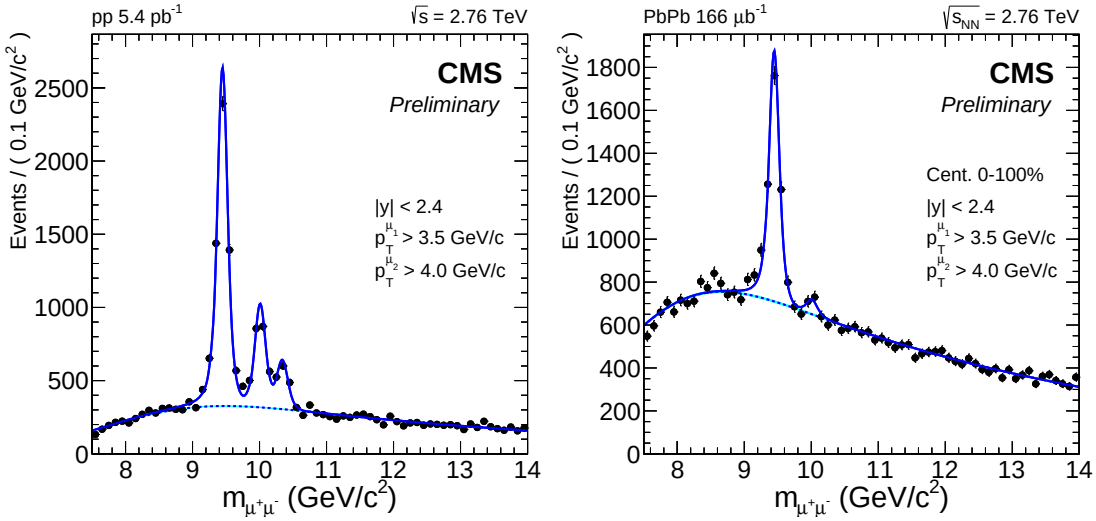

Figure 1: Dimuon invariant mass distributions from the pp (left) and PbPb (right) data at $\sqrt{s_{\mathrm{NN}}} = 2.76$ TeV, for muon pairs having one p_{T} greater than 4 GeV/c and the other greater than 3.5 GeV/c. The solid (signal + background) and dashed (background only) lines show the result of fits described in the text.

exponential function multiplied by an error function describing the low-mass turn-on, with all four parameters left free.

With one muon of p_{T} greater than 4 GeV/c and the other greater than 3.5, this fitting procedure results in $\Upsilon(1S)$ yields of 2534 ± 80 and 5014 ± 87 in PbPb and pp collisions, respectively. With both muons above 4 GeV/c, it yields 173 ± 41 for $\Upsilon(2S)$ and 7 ± 38 for $\Upsilon(3S)$ (hence unobserved) in PbPb collisions, and 1208 ± 49 for $\Upsilon(2S)$ and 619 ± 41 for $\Upsilon(3S)$ in pp collisions.

4.2 Acceptance and efficiency

In order to correct yields for the acceptance and efficiency in the PbPb analysis, the three Υ states have been simulated and embedded in PbPb events, with the same settings as in [13]. The acceptance, defined as the fraction of $\Upsilon(1S)$ mesons in the $y < |2.4|$ rapidity range that decay into muons of pseudorapidity $|\eta| < 2.4$ and p_{T} greater than 3.5 and 4 GeV/c, amounts to 35%, with a drop for the mesons of the most forward rapidity or intermediate p_{T}. For $\Upsilon(2S)$ and $\Upsilon(3S)$ where both muon p_{T} were required to be above 4 GeV/c, the acceptance is 28% for the $\Upsilon(2S)$ and 33% for the $\Upsilon(3S)$. Within this acceptance, the average reconstruction and trigger efficiencies are 66%, 72% and 75% for the $\Upsilon(1S)$, $\Upsilon(2S)$ and $\Upsilon(3S)$, respectively. The lower average $\Upsilon(1S)$ efficiency arises from including the additional decays into lower p_{T} muons, which have smaller reconstruction efficiencies, in particular near midrapidity.

The individual components of the MC efficiency are cross checked using real data and muons from J/ψ, with a technique called tag-and-probe, similar to what is described in [24]. The method consists of fitting the J/ψ candidates of the data and MC samples, with and without applying the probed selection criterion on one of the muons. The muon identification and trigger efficiency is probed by testing the trigger and muon selection response in a single-muon-triggered sample. The small observed discrepancies between the results for data and MC are used to determine p_{T} and η-dependent single muon correction factors that are applied to muons in the MC acceptance times efficiency simulation. The net correction factors to the Υ yields ranges from 3 to 16%, being stronger for low p_{T} or high rapidity. The reconstruction efficiency in the tracker is also controlled with this method by checking the presence of a track

for muons that are primarily reconstructed in the muon detectors. This check, limited by a poorer resolution and high background in the PbPb case, yields conservative 1.7% and 5.0% uncertainties for each muon, for pp and PbPb, respectively.

4.3 Systematic uncertainties

Seven line shape variations were performed to estimate the uncertainty coming from the fitting procedure. Five correspond to releasing each parameter of the signal line shape to allow for possible variations with respect to the simulated line shape. The other two line shape variations consist of using more complicated shapes for the background: by summing a first or second order Chebychev polynomial functions with the default function. These sources of uncertainty are propagated into a systematic uncertainty of maximum 28%, depending on the bin.

The systematic uncertainty coming from the acceptance and efficiency includes shape variations of the generated p_{T} and y, as well as a variation on the centrality weighting of reconstructed MC spectra. These variations are propagated into a bin-by-bin systematic uncertainty, of 2.8% and 8.2% on average in pp and PbPb respectively.

The tag-and-probe efficiency correction factors are varied within the data-driven statistical uncertainties. To do so, a hundred variations of the data-based single muon efficiencies are computed, resulting in a hundred scaling dimuon efficiency correction factors, in each analysis bin. The RMS of the resulting efficiencies is taken as a systematic uncertainty, ranging from 0.4% in pp in central rapidity bins to 17% in the most forward PbPb bins. In addition, the uncertainty on the tracking efficiency, 1.7% and 5.0% for each track, is doubled for dimuon candidates, and considered as a global uncertainty.

The uncertainties on the T_{AA} values are reported in Table 1. The uncertainty on the pp luminosity (3.7%) or PbPb number of minimum bias events (3%) are also considered as global uncertainties.

5 Results

5.1 Cross sections

Figures 2 and 3 show the differential cross sections as functions of p_{T} and rapidity, respectively. Measured yields are corrected for acceptance and efficiency, then divided by the bin width in consideration, and normalized by 1) the measured luminosity in pp collisions (left figures), 2) the number of corresponding minimum bias events times the centrality-integrated T_{AA} for the PbPb collisions (right figures), putting the two of them on a comparable scale. In pp collisions, the data allow measuring the three states with the same binning. In PbPb collisions, that same binning can be used for the $\Upsilon(1S)$, but wider bins are necessary for the $\Upsilon(2S)$. The $\Upsilon(3S)$ is not observed in PbPb collisions.

5.2 Nuclear modification factors

Nuclear modification factors, R_{AA}, are obtained by dividing the PbPb yields by the pp cross sections and T_{AA} values and are shown in Fig. 4 as a function of the Υ transverse momentum (left) and rapidity (right). The global fully-correlated systematic uncertainty includes the uncertainties in tracking efficiency, pp luminosity, PbPb minimum-bias number of events and T_{AA}. The R_{AA} results show a suppression of a factor of ≈ 2 and ≈ 10 for $\Upsilon(1S)$ and $\Upsilon(2S)$, respectively. No pronounced dependence on the meson kinematics is observed, the values being constant within uncertainties as a function of both p_{T} and y.

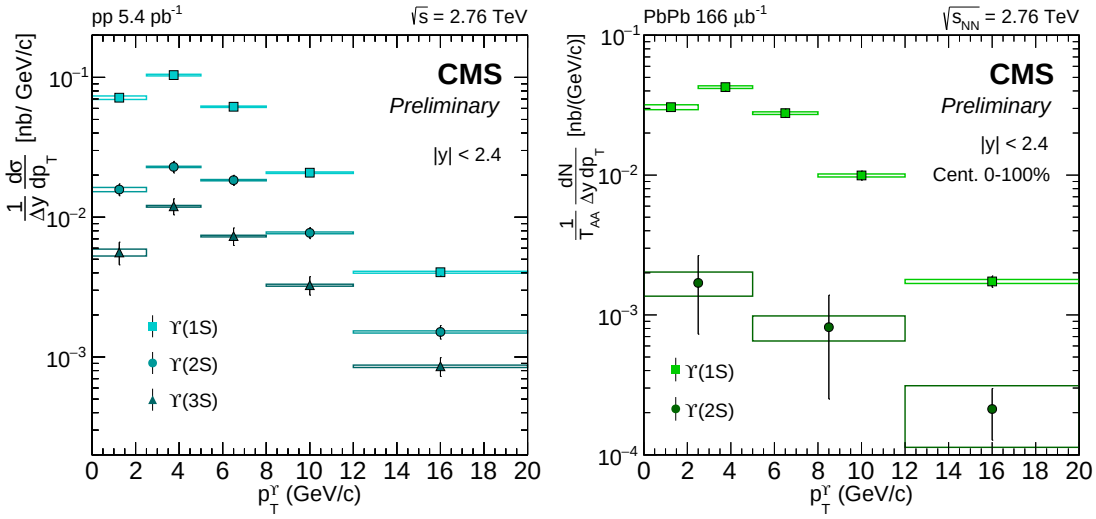

Figure 2: Differential cross section of Υ states as a function of their transverse momentum in pp (left) and PbPb (right) collisions. From top to bottom, squares, circles and triangles stand for $\Upsilon(1S)$, $\Upsilon(2S)$ and $\Upsilon(3S)$, respectively. Statistical (systematic) uncertainties are displayed as error bars (boxes). Global uncertainties of 5% (left) and 10.5% (right) are not displayed.

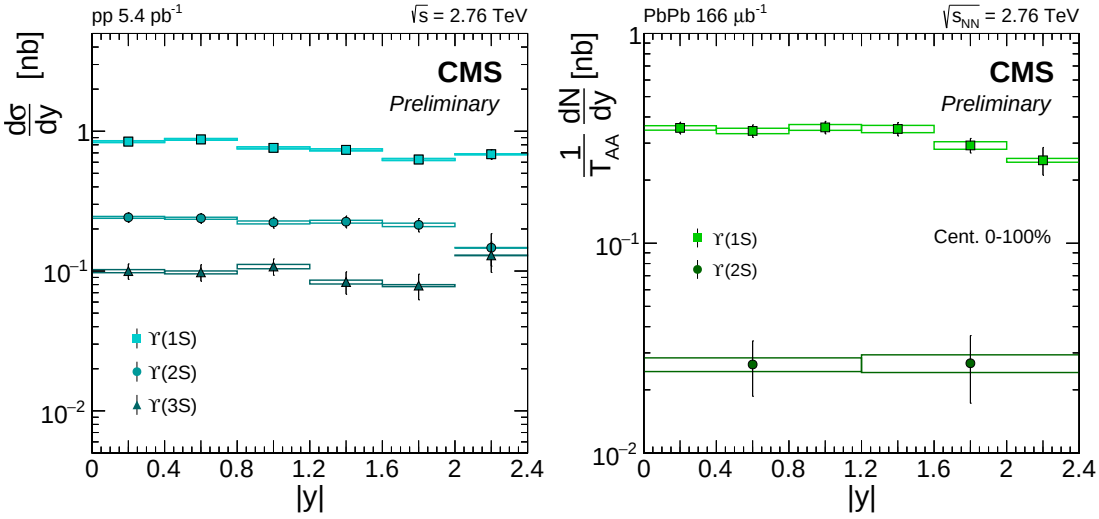

Figure 3: Differential cross section of Υ states as a function of their rapidity in pp (left) and PbPb (right) collisions. From top to bottom, squares, circles and triangles stand for $\Upsilon(1S)$, $\Upsilon(2S)$ and $\Upsilon(3S)$, respectively. Statistical (systematic) uncertainties are displayed as error bars (boxes). Global uncertainties of 5% (left) and 10.5%(right) are not displayed.

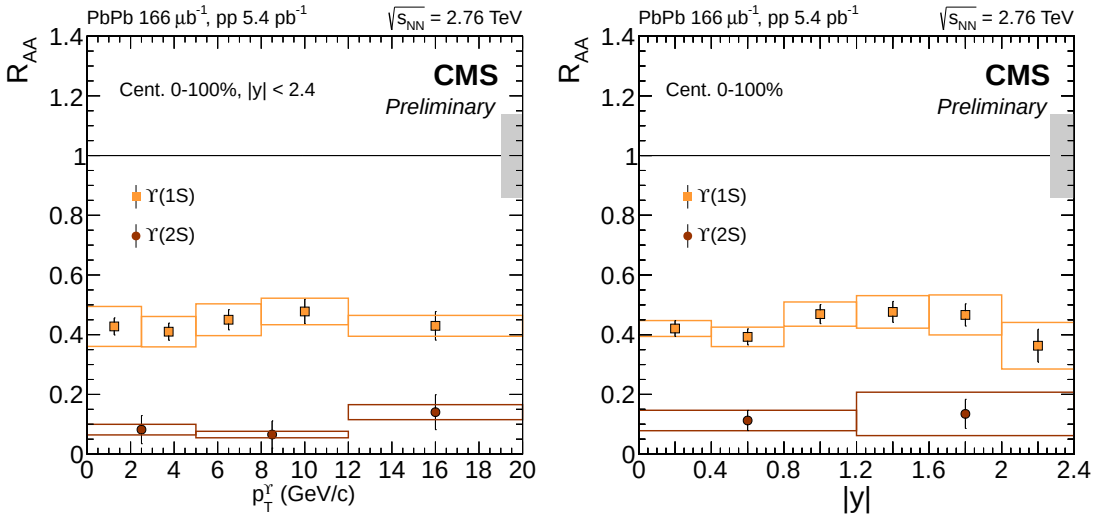

Figure 4: Nuclear modification factor of Υ(1S) and Υ(2S) in PbPb collisions as a function of transverse momentum (left) and rapidity (right). Statistical (systematic) uncertainties are displayed as error bars (boxes), while the global fully-correlated uncertainty is displayed as a box at unity.

Figure 5 shows R_{AA} as a function of centrality, displayed as the number of participating nucleons, $N_{\rm part}$. The global, fully-correlated uncertainties come from the uncertainty in the pp cross sections (which is different for the two Y states) and the PbPb tracking efficiency. The strong centrality dependence, already observed in Ref. [13], is mapped out with more precision.

The Υ(3S) not being observed, an R_{AA} upper limit is derived using the Feldman-Cousins prescription [26]. The result, together with the integrated R_{AA} values of the Υ(1S) and Υ(2S) are:

$$\begin{aligned} R_{AA}(\Upsilon(1S)) &= 0.425 \pm 0.029 \pm 0.070, \\ R_{AA}(\Upsilon(2S)) &= 0.116 \pm 0.028 \pm 0.022, \\ R_{AA}(\Upsilon(3S)) &< 0.14 \text{ at } 95\% \text{ CL}, \end{aligned}$$

with the first and second uncertainties being one-sigma statistical and systematic uncertainties, respectively.

6 Summary

The Υ(1S), Υ(2S) and Υ(3S) meson yields have been measured in PbPb and pp collisions at the same energy per nucleon pair, $\sqrt{s_{NN}} = 2.76$ TeV. The Υ(1S) and Υ(2S) are suppressed by a factor of ≈ 2 and 10, respectively, while the unobserved Υ(3S) corresponds to a suppression by a factor larger than 7, at 95% confidence level. Though a strong centrality dependence of the suppression is observed for the Υ(1S) and Υ(2S), no noticeable dependence is observed as a function of transverse momentum or rapidity.

References

[1] F. Karsch and E. Laermann, "Thermodynamics and in-medium hadron properties from lattice QCD", in *Quark-Gluon Plasma III*, R. C. Hwa and X.-N. Wang, eds. World Scientific Publishing Co. Pte. Ltd., 2004. arXiv:hep-lat/0305025.

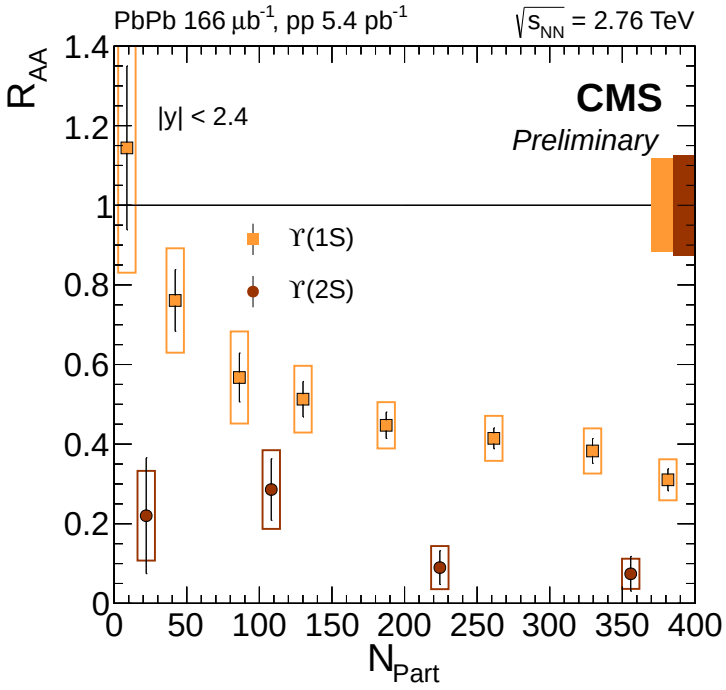

Figure 5: Nuclear modification factor of $\Upsilon(1S)$ and $\Upsilon(2S)$ in PbPb as a function of centrality, displayed as the number of participating nucleons. Statistical (systematic) uncertainties are displayed as error bars (boxes), while the global fully-correlated uncertainty is displayed as a box at unity.

[2] E. V. Shuryak, "Theory of Hadronic Plasma", *Sov. Phys. JETP* **47** (1978) 212.

[3] T. Matsui and H. Satz, "J/ψ suppression by quark-gluon plasma formation", *Phys. Lett. B* **178** (1986) 416, doi:10.1016/0370-2693(86)91404-8.

[4] Á. Mócsy and P. Petreczky, "Color screening melts quarkonium", *Phys. Rev. Lett.* **99** (2007) 211602, doi:10.1103/PhysRevLett.99.211602, arXiv:0706.2183.

[5] R. L. Thews, M. Schroedter, and J. Rafelski, "Enhanced J/ψ production in deconfined quark matter", *Phys.Rev.* **C63** (2001) 054905, doi:10.1103/PhysRevC.63.054905, arXiv:hep-ph/0007323.

[6] A. Andronic, P. Braun-Munzinger, K. Redlich, and J. Stachel, "Statistical hadronization of heavy quarks in ultra-relativistic nucleus-nucleus collisions", *Nucl.Phys.* **A789** (2007) 334–356, doi:10.1016/j.nuclphysa.2007.02.013, arXiv:nucl-th/0611023.

[7] S. Gavin and R. Vogt, "Charmonium suppression by Comover scattering in Pb + Pb collisions", *Phys.Rev.Lett.* **78** (1997) 1006–1009, doi:10.1103/PhysRevLett.78.1006, arXiv:hep-ph/9606460.

[8] A. Capella, A. Kaidalov, A. Kouider Akil, and C. Gerschel, "J / psi and psi-prime suppression in heavy ion collisions", *Phys.Lett.* **B393** (1997) 431–436, doi:10.1016/S0370-2693(96)01650-4, arXiv:hep-ph/9607265.

[9] R. Vogt, "Cold Nuclear Matter Effects on J/ψ and Y Production at energies available at the CERN Large Hadron Collider (LHC)", *Phys. Rev. C* **81** (2010) 044903, doi:10.1103/PhysRevC.81.044903, arXiv:1003.3497.

[10] A. Emerick, X. Zhao, and R. Rapp, "Bottomonia in the Quark-Gluon Plasma and their Production at RHIC and LHC", *Eur.Phys.J.* **A48** (2012) 72, doi:10.1140/epja/i2012-12072-y, arXiv:1111.6537.

[11] CMS Collaboration, "Suppression of non-prompt J/ψ, prompt J/ψ, and Y(1S) in PbPb collisions at $\sqrt{s_{NN}} = 2.76$ TeV", *JHEP* **1205** (2012) 063, doi:10.1007/JHEP05(2012)063, arXiv:1201.5069.

[12] CMS Collaboration, "Indications of suppression of excited Y states in PbPb collisions at $\sqrt{S_{NN}}$ = 2.76 TeV", *Phys.Rev.Lett.* **107** (2011) 052302, doi:10.1103/PhysRevLett.107.052302, arXiv:1105.4894.

[13] CMS Collaboration, "Observation of sequential Upsilon suppression in PbPb collisions", *Phys.Rev.Lett.* **109** (2012) 222301, doi:10.1103/PhysRevLett.109.222301, arXiv:1208.2826.

[14] ALICE Collaboration, "Production of inclusive Y(1S) and Y(2S) in p-Pb collisions at $\sqrt{\mathbf{s}_{\mathrm{NN}}} = \mathbf{5.02}$ TeV", *Phys.Lett.* **B740** (2014) 105, doi:10.1016/j.physletb.2014.11.041, arXiv:1410.2234.

[15] LHCb Collaboration, "Study of Y production and cold nuclear matter effects in pPb collisions at $\sqrt{s_{NN}}$=5 TeV", *JHEP* **1407** (2014) 094, doi:10.1007/JHEP07(2014)094, arXiv:1405.5152.

[16] CMS Collaboration, "Event activity dependence of Y(nS) production in $\sqrt{s_{NN}}$=5.02 TeV pPb and $\sqrt{s}$=2.76 TeV pp collisions", *JHEP* **1404** (2014) 103, doi:10.1007/JHEP04(2014)103, arXiv:1312.6300.

[17] CMS Collaboration, "The CMS experiment at the CERN LHC", *JINST* **3** (2008) S08004, doi:10.1088/1748-0221/3/08/S08004.

[18] CMS Collaboration, "Measurement of momentum scale and resolution using low-mass resonances and cosmic ray muons", CMS Physics Analysis Summary TRK-2010/004, 2010.

[19] CMS Collaboration, "Observation and studies of jet quenching in PbPb collisions at nucleon-nucleon center-of-mass energy = 2.76 TeV", *Phys.Rev.* **C84** (2011) 024906, doi:10.1103/PhysRevC.84.024906, arXiv:1102.1957.

[20] CMS Collaboration, "Luminosity Calibration for the 2013 Proton-Lead and Proton-Proton Data Taking", CMS Physics Analysis Summary CMS-PAS-LUM-13-002, 2013.

[21] M. L. Miller, K. Reygers, S. J. Sanders, and P. Steinberg, "Glauber modeling in high-energy nuclear collisions", *Ann. Rev. Nucl. Part. Sci.* **57** (2007) 205, doi:10.1146/annurev.nucl.57.090506.123020, arXiv:nucl-ex/0701025.

[22] CMS Collaboration, "Performance of CMS muon reconstruction in pp collision events at $\sqrt{s} = 7$ TeV", *JINST* **7** (2012) P10002, doi:10.1088/1748-0221/7/10/P10002, arXiv:1206.4071.

[23] M. J. Oreglia, "A Study of the Reactions $\psi' \to \gamma\gamma\psi$", *Ph.D. Thesis* (1980) Appendix D.

[24] CMS Collaboration, "Measurement of the $\Upsilon(1S)$, $\Upsilon(2S)$, and $\Upsilon(3S)$ cross sections in pp collisions at $\sqrt{s}$ = 7 TeV", *Phys.Lett.* **B727** (2013) 101–125, doi:10.1016/j.physletb.2013.10.033, arXiv:1303.5900.

[25] Particle Data Group Collaboration, "Review of Particle Physics", *Chin.Phys.* **C38** (2014) 090001, doi:10.1088/1674-1137/38/9/090001.

[26] G. J. Feldman and R. D. Cousins, "A Unified approach to the classical statistical analysis of small signals", *Phys.Rev.* **D57** (1998) 3873–3889, doi:10.1103/PhysRevD.57.3873, arXiv:physics/9711021.